Research Square

Preprints are preliminary reports that have not undergone peer review.
They should not be considered conclusive, used to inform clinical practice,
or referenced by the media as validated information.

A Chromene-Based Fluorescent Probe for Rapid Hypochlorite Detection in Environmental Matrices, Plant Tissues, and a Smartphone Platform

Guangqin Gao
Henan Agricultural University
Baixue Zhao
Henan Agricultural University
Yuli Dang
Henan Agricultural University
Wenbo Shen
Henan Agricultural University
Zhanqi Cao
Henan Agricultural University
Chenyu Li
Henan Agricultural University
Rubing Feng
Henan Agricultural University
Puhui Xie
phxie2013@163.com
Henan Agricultural University
Fengqi Guo
Zhengzhou University

Research Article

Keywords: Fluorescent probe, Hypochlorite detection, Chromene, Environmental monitoring, Plant imaging, Smartphone-based portable analysis

Posted Date: June 30th, 2026

DOI: https://doi.org/10.21203/rs.3.rs-10006895/v1

License: This work is licensed under a Creative Commons Attribution 4.0 International License.
Read Full License

Additional Declarations: No competing interests reported.

Abstract

Hypochlorite (ClO^-) plays important roles in maintaining physiological homeostasis. However, elevated level of ClO^- poses significant risks to both human health and the environment, and rapid on-site detection remains challenging. In this work, a known chromene-based fluorescent probe (1), originally recognizing nitric oxide in DMSO-PBS buffer, was found to respond selectively to ClO^- when tested in an ethanol-water (1:1, v/v) medium. Under these conditions, the probe exhibited a rapid turn-on fluorescence response at 530 nm within 30 seconds upon exposure to ClO^-. Probe **1** showed properties in detecting ClO^- with high sensitivity (limit of detection 11 nM), excellent selectivity over other analytes, good stability across pH 4–10, and a broad linear range (0–170 μM). Mechanistic studies confirmed that ClO^- triggers oxidative cleavage of the imine bond, regenerating the strongly fluorescent aldehyde **1A**. Based on this response, we developed a smartphone-based portable platform for accurate ClO^- quantification in real water samples with recoveries of 97.4–104.2%. The probe was further validated for ClO^- detection in diverse applications, including soil samples, living plant seedings, microfluidic devices, and real-time monitoring in plant cells. This work provides a rapid and portable tool for ClO^- monitoring across environmental and biological matrices, effectively expanding the functionality of a single molecular platform.

1 Introduction

Hypochlorite (ClO^-) is a low-cost, potent oxidant widely used as a disinfectant and in industrial processes including textile bleaching, cyanide effluent remediation, pulp processing, chemical synthesis, membrane bioreactor sterilization, and wastewater disinfection [1, 2]. However, residual ClO^- in water poses health risks by generating toxic byproducts, such as trihalomethanes [3–5]. As a key reactive oxygen species (ROS), ClO^- mediates essential biological functions through antimicrobial and anti-inflammatory actions. It supports host defense by eliminating pathogens and serves as a critical antimicrobial oxidant in pathogen response, autoimmunity, and pathophysiology [6–11]. Conversely, misregulation leading to aberrant ClO^- concentrations triggers tissue damage and contributes to pathologies including ischemic stroke, Huntington's, Parkinson's, and Alzheimer's diseases [12, 13], with toxicity further evidenced by sodium hypochlorite's murine oral LD_{50} of 5.8 g/kg [14]. Consequently, stringent regulation of intracellular ClO^- levels is crucial for maintaining physiological homeostasis and preventing cytotoxicity.

Given its vital roles and significant toxicity when dysregulated, tracking ClO^- across environmental and biological systems requires robust analytical tools. While established techniques such as voltammetry, spectroscopy, chemiluminescence, electrochemistry, and chromatography enable ClO^- detection [15–19], they often entail complex sample pretreatment, costly instrumentation, time-consuming procedures, and specialized operation. In contrast, fluorescence probes have emerged as a compelling alternative, offering ultra-high sensitivity, real-time monitoring potential, non-invasive spatial resolution, and minimal

sample preparation requirements [20–22]. Notably, turn-on fluorescence probes provide superior sensitivity and signal discrimination compared to quenching-based designs [23, 24]. As a complement to precise fluorescence quantification, the development of portable platforms enabling semi-quantitative visual assessment is crucial for practical field deployment, offering enhanced convenience and reliability. With their high-resolution cameras and processing capabilities, smartphones represent a promising solution, utilizing red-green-blue (RGB) analysis to achieve colorimetric detection of ClO^- [25–27]. This approach enables rapid on-site quantification, eliminating the need for complex pretreatment or costly instrumentation.

Most existing probes are designed to target a single analyte with high selectivity [28–34]. Developing a single molecular platform that can selectively detect different analytes under tunable conditions remains an intriguing challenge. Such a versatile probe would not only simplify synthetic efforts but also provide a unique opportunity to investigate the interplay between multiple analytes in complex biological or environmental systems. We previously reported that probe **1**, 2-((7-(diethylamino)-2H-chromen-3-yl)methyleneamino)-3-aminomaleonitrile, exhibits spectroscopic response toward nitric oxide (NO) in DMSO-PBS (1:9, v/v, pH 7.4, 10 mM), with a fluorescence enhancement at 500 nm within 2 min [35]. This response arose from NO-induced intramolecular oxidative cyclization, which generated 2-(7-(diethylamino)-2H-chromen-3-yl)-1H-imidazole-4,5-dicarbonitrile and thereby enabled real-time imaging of NO in living cells. In the present study, we discovered that simply altering the detection medium to EtOH-H_2O (1:1, v/v) switches the selectivity of probe **1** toward ClO^-. Under these conditions, probe **1** exhibits a fluorescence enhancement at 530 nm within 30 s upon addition of ClO^-, with excellent selectivity over other competitive analytes. The EtOH-H_2O medium offers good solubility for both the probe and ClO^- sources, while providing a compatible environment for applications such as real water sample analysis and cellular imaging. Thus, the spectral properties of probe **1** toward ClO^- in EtOH-H_2O (1:1, v/v), including selectivity, sensitivity, response time, mechanism, and pH dependence were investigated. Furthermore, the practical utility of this probe is demonstrated across diverse applications: (i) environmental monitoring in soil, in vivo plant tissues and real water samples using a smartphone-based RGB analysis platform; (ii) biological imaging of exogenous ClO^- in living cells; and (iii) recognizing ClO^- using agar membrane-based and filter paper-based microfluidic systems. This work not only expands the application scope of probe **1** but also provides a simple, versatile tool for ClO^- detection across environmental and biological fields.

2 Experimental

2.1 Instruments and general methods

^1H NMR and ^{13}C NMR spectra were determined on a Bruker BioSpin GmbH spectrometer with frequencies of 400 MHz for proton spectra and 101 MHz for carbon spectra. Mass spectra were detected on a Bruker Daltonics Autoflex IITM MALDI TOF MS spectrometer. The optical spectra of UV –

vis absorption and fluorescence spectra were determined with a on TU-1901 spectrometer and a VARIAN Cary Eclipse spectrophotometer, respectively. The absolute fluorescence quantum yields were measured on a Hamamatsu C11347 absolute photoluminescence quantum yield measurement system and a U6039-05 PLQY measurement software. The fluorescence decays were acquired with a Quantaurus-Tau fluorescence lifetime measurement system (C11367, Hamamatsu Photonics Co., Japan) and a U11487-01 software for controlling and calculating the fluorescence lifetime. The pH values were recorded on PHS-3C pH meter. Fluorescence imaging of plant cells was observed using a Nikon Ti2 A1HD25 high-resolution laser confocal microscope. Lyophilization was conducted using an 18N freeze dryer, from LICHEN Science and Technology. PRX-450D intelligent artificial climate chambers were used to cultivate plant seedlings. Confocal fluorescence images were acquired using a Nikon Ti2-A1 HD25 microscope with NIS-Elements AR software, employing a 20× water immersion objective. Details in synthesis and characterization of probe **1**, ROS preparation, extraction of protoplasts from *Paulownia* leaf cells, and Statistical method can be found in our previous paper [35].

2.2 Preparation of solutions and spectral measurements

Stock solution of probe **1** (1 mM) was prepared in ethanol. Stock solutions of analytes were prepared in distilled water for the following: ROS (10 mM), including H_2O_2, ClO^-, $O_2^{-\bullet}$, $HO^\bullet$, $^1O_2$, NO, and $ONOO^-$; common anions (10 mM) from their potassium or sodium salts, including F^-, Cl^-, Br^-, I^-, S^{2-}, ClO_3^-, NO_3^-, NO_2^-, SO_4^{2-}, SO_3^{2-}, $S_2O_3^{2-}$ and PO_4^{3-}; and biothiols (5 mM), including Cys, Hcy, and GSH. Absorption and fluorescence spectra were measured by adding aliquots of each analyte (10 eq) to probe **1** (10 μM) in EtOH-H_2O (1:1, v/v) to assess spectral selectivity. The spectroscopic titration experiments were performed upon adding aliquots of ClO^- stock solution to probe **1** (10 μM) in EtOH-H_2O (1:1, v/v), after the reactions were conducted at room temperature for 30 s, the absorption and fluorescence spectra were recorded.

2.3 Smartphone-based fluorescent measurement for ClO^-

Samples were prepared containing probe **1** (10 μM) and ClO^- at varying concentrations (C_{ClO^-}, μM) of 0, 20, 40, 60, 80, 100, 120, 140, 160, and 180 in EtOH-H_2O (1:1, v/v). The sample tubes were illuminated with 365 nm UV light at a 3 cm distance in a dark environment, and fluorescence images were captured using a smartphone's camera, from which RGB values were extracted with a Color Recognizer application. To evaluate the reliability and practicality of the smartphone-based semiquantitative detection, a calibration curve was established by plotting the Euclidean distance between the RGB values of each sample and those of the control against the ClO^- concentration. The Euclidean distance was calculated using the following equation [36]:

The subscripts x and 0 indicate the RGB values for the probe with and without ClO^-, respectively.

2.4 Determination of ClO^- in real water samples

Real water samples (tap water, Longzi Lake water, and purified water) were collected to evaluate the practical application of probe **1**. Tap water was obtained from our laboratory. Longzi Lake water was filtered through a 0.22 μm filter paper to remove impurities prior to use. Purified water was purchased from a local supermarket. Each water sample was mixed with EtOH in a 1:1 (v/v) ratio. To the resulting EtOH-water solution, varying volumes of a stock ClO^- solution were added to achieve final concentrations of 20, 60, and 100 μM for spiked samples. Probe **1** was then added at a final concentration of 10 μM. After 30 s, RGB values were acquired and the concentrations of ClO^- were calculated from the calibration curve. Three replicate experiments were conducted for each sample.

2.5 Applications of probe 1 in ClO^- recognition on various matrixes

The feasibility of applying probe **1** for ClO^- detection was tested on various substrates, including soil, filter paper, agar membranes, and *in vivo* plants. For application in soil, commercial potting soil samples were treated with probe **1** (10 μM, EtOH-H_2O 1:1 v/v) for 2 hours. Subsequently, ClO^- solution (50 μM) was introduced to the soil. Dipstick assays for ClO^- were conducted using paper-based and agar membrane-based microfluidic devices. For filter paper-based microfluidic devices, medium-speed qualitative filter paper discs were cut into 1.5 cm diameter pieces, shaped into pentagrams, and immersed in 10 mL of probe **1** solution (10 μM, EtOH-H_2O, 1:1 v/v) for 24 hours. The pentagrams were then retrieved with tweezers and freeze-dried for subsequent detection for ClO^-. For agar membrane-based microfluidic devices, 100 mg of agarose powder was dissolved in 10 mL deionized water at 120°C. Subsequently, 200 μL of the hot agarose solution was rapidly transferred to a 0.5-mL centrifuge tube and incubated at 4°C for 30 minutes. After hydrogel formation at the tube bottom, probe **1** solution (10 μM, EtOH-H_2O, 1:1 v/v) was injected through the tube orifice. Finally, the conical base section was excised to obtain an agar membrane measuring 5 mm in thickness and 3 mm in diameter. Followed by air-drying and subsequent exposure to ClO^- solutions and drying, the substrates of soil, filter paper, and agar membranes were photographed under 365 nm UV illumination.

The plants seedings, including paulownia, bok choy, mung bean, soybean, corn, and wheat seedings, were respectively obtained from hydroponically cultured in controlled-climate chambers. Following 4-hour aqueous pretreatment, the seeding samples were treated with ClO^- solution (50 μM) for 4 hours, then the samples were transferred to aqueous medium containing probe **1** (10 μM in EtOH-H_2O, 1:1 v/v) for further 4-hour incubation. Then the samples were imaged under irradiation of a 365 nm UV lamp.

2.6 Confocal fluorescence imaging

Twenty-day-old *Paulownia* saplings were transferred to culture dishes and incubated with probe **1** (10 μM) for 4 hours, followed by treatment with ClO^- solution (100 μM) for an additional 4 hours. For protoplast imaging, protoplasts were first pretreated with probe **1** (10 μM) and then exposed to ClO^- (100 μM). Prior to confocal imaging, the incubation media were removed, and the samples were washed three times with PBS (pH 7.4), then transferred to 35 mm glass-bottom confocal dishes. Super-resolution

fluorescence images of root tip cells were acquired every 1 hour over a total period of 4 hours, while protoplast images were acquired every 10 minutes over a total period of 40 minutes. All experiments were performed in triplicate (n ≥ 3).

3 Results and Discussion

3.1 Design of probe

In probe **1**, the diethylamino moiety serves as a strong electron-donating group, while the nitrile groups in the aminomaleonitrile unit act as electron-withdrawing groups. This donor–acceptor character, together with extended π-π conjugation, enables fluorescence emission in the red spectral region through efficient intramolecular charge transfer (ICT) induced by the electron push-pull system. However, molecules containing C = N bonds are typically nonfluorescent or weakly fluorescent because the *cis-trans* isomerization of the C = N bond serves as the predominant nonradiative decay pathway from the excited state to the ground state [37]. To address this, we designed probe **1** with a C = N bond that can be selectively cleaved or structurally locked upon analyte recognition, thereby suppressing isomerization and restoring fluorescence. Specifically, significant fluorescence enhancement can be achieved either via the formation of a covalently bridged C = N structure or through direct cleavage of the C = N bond, both of which inhibit the nonradiative isomerization pathway. The former mode was previously observed in the selective recognition of NO in DMSO-PBS medium [35], whereas in this work, we exploit the latter mechanism: direct cleavage of the C = N bond by ClO^- in EtOH-H_2O medium (Scheme 1). This disruption of the isomerization pathway restores the ICT process, leading to a turn-on fluorescence response.

3.2 The specificity of 1 towards ClO^-

Upon addition of each analyte (100 μM), including reactive oxygen species (ClO^-, H_2O_2, $ONOO^-$, $HO^•$, NO, $^1O_2$, $O_2^{-•}$), biothiols (Cys, Hcy, and GSH), and common anions (F^-, Cl^-, Br^-, I^-, S^{2-}, ClO_3^-, NO_3^-, NO_2^-, SO_4^{2-}, SO_3^{2-}, $S_2O_3^{2-}$ and PO_4^{3-}) to a solution of probe **1** (10 μM) in EtOH-H_2O (1:1, v/v), the absorption and fluorescence spectra were immediately recorded. Probe **1** displayed a low-energy absorption peak centered at 480 nm, attributed to the S_0 to S_1 transition. Upon addition of ClO^-, the absorbance at this wavelength decreased significantly (Fig. 1a), whereas other tested analytes caused no obvious change.

The fluorescence of probe **1** alone was rather weak, with an emission maximum at 582 nm and a quantum yield (Φ) of 2%, likely due to *cis-trans* isomerization of the Schiff base moiety. In our previous work, upon recognition of NO in DMSO-PBS medium, probe **1** exhibited a fluorescence enhancement at 500 nm with bluish-green emission under 365 nm UV light. In the present study focusing on ClO^- detection in EtOH-H_2O (1:1, v/v), a distinct response was observed: upon addition of ClO^-, a 17-fold fluorescence enhancement occurred at 530 nm (Φ = 38%) with a blue-shift of 52 nm, accompanied by a visible yellowish-green emission (Fig. 1b insert). Importantly, other analytes, including NO, did not

significantly alter the fluorescence under these aqueous conditions, demonstrating that probe **1** exhibits high selectivity toward ClO^- in the EtOH-H_2O medium.

To further evaluate the selectivity and practical applicability of probe **1**, competitive experiments were conducted to assess its anti-interference performance toward ClO^-. As shown in Fig. 1c, no significant changes in fluorescence of probe **1** (10 μM) were observed after the addition of different analytes (100 μM) including H_2O_2, $ONOO^-$, $HO^•$, NO, $^1O_2$, $O_2^{-•}$, Cys, Hcy, GSH, F^-, Cl^-, Br^-, I^-, S^{2-}, ClO_3^-, NO_3^-, NO_2^-, SO_4^{2-}, SO_3^{2-}, $S_2O_3^{2-}$ and PO_4^{3-}. On the contrary, only the addition of ClO^- to probe **1** solution resulted in a significant increase in fluorescence intensity at 535 nm. Besides, no significant variation in fluorescence intensity was observed upon the addition of ClO^- to probe **1** in the presence of other tested analytes under identical conditions, indicating that probe **1** possesses good anti-interference ability for ClO^- detection.

The effect of pH on the sensing performance was also investigated, as a suitable pH range is critical for environmental applications. As shown in Fig. 1d and Figs. S1–S2, the absorption spectra and fluorescence intensity of probe **1** at 582 nm remained stable over a wide pH range of 4.0–10.0, indicating good stability under both acidic and basic conditions. Upon addition of ClO^- (10 equiv.), a significant fluorescence enhancement (17-fold) at 530 nm was observed across the entire pH range tested. These results demonstrate that probe **1** can function effectively as a fluorescent sensor for ClO^- over a broad pH window.

To assess the response rate of probe **1** toward ClO^-, time-dependent fluorescence measurements were performed in EtOH-H_2O (1:1, v/v) solution. Upon addition of ClO^- (10 equiv.), a rapid fluorescence enhancement of probe **1** was observed, reaching a maximum within 30 s (Fig. S3). This fast response suggests that probe **1** is suitable for real-time monitoring of ClO^-. Accordingly, all subsequent spectroscopic measurements were conducted after a 30 s incubation at room temperature.

3.3 Spectral sensitivities of 1 toward ClO^-

To investigate the spectroscopic sensitivity of **1** toward ClO^-, the absorption and fluorescence spectra are conducted upon the titration of ClO^- to the solution of **1** (Fig. 2a and Fig. 2c). As ClO^- concentration increased (0–170 μM), probe **1** exhibited decreased absorbance at 480 nm accompanied by a blue-shift to 455 nm (Fig. 2a). Concurrently, new shoulders emerged at 365 and 575 nm, and three isosbestic points formed at 345, 400, and 538 nm. Over 0–30 μM ClO^-, absorbance at 480 nm exhibited a linear relationship ($y = -5048.2128x + 0.4704$, $R^2 = 0.9947$, Fig. 2b). The LOD for ClO^- was calculated as 0.89 μM using the 3σ/k criterion, where σ = 0.0015 (standard deviation of 11 blanks) and k = − 5048.2128 (slope) [38]. The fluorescence emission peak of **1** gradually blue-shifted to 530 nm with increasing ClO^- concentration, while intensity increased (Fig. 2c). A linear relationship ($y = 5.2412\times10^2x - 16.3475$; $R^2 = 0.9972$) was observed between fluorescence intensity at 530 nm and ClO^- concentration (0–170 μM, Fig. 2d). Using the 3σ/k criterion, the LOD for ClO^- was calculated as 11 nM, which is much lower than those

of other fluorescent sensors reported for ClO^- (Table 1). These results implied that sensitive and quantitative analysis of ClO^- in broad concentration range could be possible by using probe **1** as a fluorescent sensor.

3.4 Recognition mechanisms

Unlike our previous work on NO recognition in DMSO-PBS, which relied on the formation of a covalently bridged C = N structure, the present study demonstrates a distinct mechanism: ClO^- triggers direct oxidative cleavage of the imine bond, regenerating the strongly fluorescent 7-(diethylamino)-2H-chromene-3-carbaldehyde (**1A**) (Scheme 1), as confirmed by HR-MS, absorption, ^1H NMR, and DFT calculations. HR-MS analysis of the **1** + ClO^- mixture (Fig. S4) showed a peak at *m/z* 233.1330, matching the theoretical value of $[M + H]^+$ for **1A**. Both **1A** and the **1** + ClO^- mixture exhibited the same absorption maximum at 410 nm (Fig. S5). Partial ^1H NMR comparison of **1** + ClO^- revealed the appearance of a signal at 9.35 ppm in the reaction mixture (Fig. 3a), attributable to the aldehyde proton of **1A**; other labeled signals in the spectrum also corresponded to protons of **1A**, further confirming ClO^--triggered oxidative cleavage of the C = N bond to regenerate the aldehyde group. Similar mechanisms have also been reported in the literature [39, 40]. In probe **1**, free rotation of the C–N single bond adjacent to the imine nitrogen promotes nonradiative decay of the excited state [41], resulting in weak fluorescence at 582 nm. Upon reaction with ClO^-, the C = N bond in probe **1** is cleaved, which suppresses C = N isomerization and leads to the formation of **1A**. As a result, strong fluorescence emission at 530 nm is observed. Lifetime measurements (Fig. S6) show that the fluorescence lifetime (τ) is 1.15 ns for **1**, which increases to 2.36 ns upon reaction with ClO^- (**1** + ClO^-). The shorter lifetime and lower quantum yield (Φ) of **1** indicate that non-radiative decay via C = N isomerization is the dominant relaxation pathway. This is supported by the calculated non-radiative decay rate ($k_{nr} = (1-\Phi_F)/\tau_F$), which is 8.52×10^8 s^{-1} for **1**, significantly larger than its radiative decay rate ($k_r = \Phi_F/\tau_F$) of 1.74×10^7 s^{-1}). These results confirm that the excited state of probe **1** undergoes much more efficient non-radiative decay [42].

To elucidate the response mechanism of probe **1** toward ClO^-, density functional theory (DFT) calculations were performed at the B3LYP/6-31G level using Gaussian 09. The HOMO and LUMO distributions of **1** and **1A** are shown in Fig. 3b. In probe **1**, the HOMO electron density is primarily localized on the chromene ring unit, while the LUMO resides predominantly on the maleonitrile-imine moiety. This spatial separation facilitates ICT from HOMO to LUMO. The extended π-delocalization across the conjugated C = N bridge yields a narrower HOMO–LUMO gap (2.8945 eV), consistent with the observed long-wavelength absorption at 480 nm. In contrast, **1A** exhibits a significantly higher LUMO energy level and reduced π-conjugation. The wider energy gap (3.3457 eV) explains the blue-shifted absorption (410 nm). The shortened π-system in **1A** facilitates strong green fluorescence at 530 nm.

3.5 Monitoring ClO^- in real water samples on smartphone

The smartphone sensing platform eliminates the need for large instruments such as a fluorescence spectrometer, making it convenient, time-saving, and cost-effective. For this reason, the turn-on

fluorescence changes of probe **1** toward ClO^- was transferred into digital information, using an intelligent detection platform setup by a smartphone with a Color Recognizer application and a portable 365 nm UV lamp, for on-site quantitatively analyzing ClO^- [43, 44]. By using this platform, fluorescent photographs of **1** (10 μM) with different ClO^- concentrations under 365 nm radiation were respectively captured. At the same time, the obtained images were digitized to RGB data. After collecting and analyzing the RGB data, the calibration curve was established. Fitting the relationship between the Euclidean distances and ClO^- concentrations (0–140 μM) displays a good linear relationship of $y = 2.82 + 7.71 \cdot 10^5 x$ ($R^2 = 0.9970$, Fig. S7, Table S1 and Fig. 4). The detection limits were 67 nM for ClO^-. These results indicated that **1** was capable of instant and quantitative sensing ClO^- via an auxiliary equipment of smartphone, with easy portability, high reliability and sensitivity.

Using the as-constructed calibration curve between the Euclidean distance and the ClO^- concentrations as well as the spike-and-recovery method, ClO^- in real water samples (tap water, Longzi lake water, and purified water) were detected to further verify the ability of the probe (10.0 μM) for accurately, quickly, and sensitively detecting ClO^-. The concentration of ClO^- in tap water, Longzi Lake and purified water were measured to be 0.14 μM, 0.48 μM and 0.00 μM, respectively. After different concentrations (20, 60, and 100 μM) of ClO^- were respectively added to probe **1** in EtOH-H_2O (1:1, v/v), the actual concentration of ClO^- was measured. Reliable recoveries of 97.4–104.2% with relative standard deviations (RSDs) of 1.3–4.1% were resulted (Table 2). These results indicated that the on-site measurement of the ClO^- content with probe **1** could be easily achieved with good precision and recoveries through the portable smartphone-based platform, which broadened the application range of the fluorescent probe for ClO^-.

Table 2

Determination of ClO^- in actual water samples by using **1** (10 μM) in EtOH-water (1:1, v/v) and a smartphone-based method.

Samples	Spiked (μM)	Detected (μM)	Recovery (%)	RSD (%, n = 3)
Tap water	0	0.14		
	20	20.98	104.2	3.1
	60	62.33	103.7	2.5
	100	98.65	98.5	1.8
Lake water	0	0.48		
	20	20.66	100.9	4.1
	60	62.72	103.7	3.7
	100	98.83	98.2	1.6
Purified water	0	0.00		
	20	20.23	101.2	2.4
	60	59.38	99.0	1.3
	100	97.37	97.4	2.1

3.6 Applications in ClO^- recognition on diverse matrixes

To facilitate simple, rapid ClO^- detection, we developed two portable platforms, pentagram-shaped test strips and agarose gel membranes. For test strips: under UV illumination, blank paper exhibited blue emission of background interference, which was significantly suppressed upon pretreatment with probe **1**. Exposure to increasing ClO^- concentrations triggered a distinct green emission transition in probe-treated strips, with fluorescence intensity positively correlating with ClO^- levels (Fig. 5a). For agarose gel membranes, the blank films showed no inherent emission under UV. Probe pretreatment induced weak dark-blue emission, suggesting probe-agar interactions. When exposed to ClO^-, these films underwent a marked blue-to-green fluorescence shift, exhibiting dose-dependent fluorescence enhancement (Fig. 5b). Both systems enable rapid visual semi-quantification of ClO^-, with agarose gel films further demonstrating functionality in complex matrices. The advantages of such portable platforms with ultra-low cost, portability, simplicity, environmental compatibility, rapid response, and minimal sample requirements highlight its potential for integration into microfluidic paper-based and film-based analytical devices for point-of-care applications in resource-limited settings.

To further assess the practical utility of probe **1**, we evaluated the performance of **1** for visualization ClO^- on diverse substrates, including soil and seedlings of various plant species such as paulownia, bok choy, mung bean, soybean, corn, and wheat. Samples were pretreated by soaking in probe **1** solution (50.0 μM) followed by air drying. As shown in Fig. 5c, all probe-treated substrates including soil and seedlings exhibited very weak initial fluorescence under UV light. However, subsequent exposure to 10 equivalents of ClO^- triggered a distinct green emission across all samples. This clear turn-on fluorescence demonstrates the successful recognition of ClO^- using probe **1** on these complex matrices. These results highlight the potential of **1** as a practical sensor for identifying ClO^- contamination in environmental and agricultural samples like soil and diverse plant seedlings.

3.7 Applications of real-time monitoring ClO^- in plant cells

In our previous study, the minimum cytotoxicity of this probe to *Paulownia* cells has been demonstrated [35]. Thus, we employed probe **1** and *Paulownia* as a model system to evaluate ClO^- levels in plant cells via fluorescence imaging. First, we assessed the ability of probe **1** to image exogenous ClO^- in real-time within root tip cells. The cells pretreated with probe **1** (10 μM) were incubated with ClO^- (100 μM), and fluorescence images were captured hourly over 4 hours. With prolonged incubation, the red-channel fluorescence (basal signal from probe **1**) progressively attenuated, while the green-channel fluorescence (indicating ClO^- detection) intensified concurrently (Fig. 6a,b). Next, we verified real-time imaging capability of probe **1** in leaf protoplasts. Following pretreatment with probe **1** (10 μM), protoplasts were exposed to ClO^- (100 μM), and ClO^- levels were monitored at 10-minute intervals for 40 minutes. Similarly, the red-channel signal (basal fluorescence) decreased time-dependently, while the green-channel signal (ClO^- detection) increased correspondingly (Fig. 6c,d). These results demonstrate probe reliability for real-time monitoring of elevated ClO^- levels. In both root tip cells and leaf protoplasts, the red-channel fluorescence (probe signal) and green-channel fluorescence (ClO^- response) consistently exhibited an inverse relationship in intensity. Furthermore, the specific fluorescence responses of probe **1** to ClO^- reveal the dynamics of ClO^- accumulation in living plants.

4 Conclusion

In summary, a chromene-based fluorescent probe **1** was developed for turn-on fluorescence detection of ClO^- via C = N bond oxidative cleavage in media of EtOH-H_2O. The probe shows low detection limit (11 nM), fast response (≤ 30 s), broad pH tolerance (4–10), and a wide linear range (0–170 μM). A smartphone-based platform enabled successful quantification of ClO^- in various environmental water samples, demonstrating its practical utility for portable and on-site ClO^- monitoring. Besides, the probe was further validated for ClO^- detection in diverse applications, including soil samples, living plant seedlings, microfluidic devices, and real-time monitoring in plant cells. This work demonstrates how simply changing the detection medium can expand the functionality of a single molecular platform for different analytes.

Declarations

Declaration of competing interest

The authors declare that they have no known competing financial interests or personal relationships that could have appeared to influence the work reported in this paper.

Author Contribution

Guangqin Gao: Writing – original draft, Funding acquisition, Investigation, Conceptualization, Formal analysis, Data curation, Methodology, Project administration. Baixue Zhao: Formal analysis, Data curation, Methodology. Yuli Dang: Visualization, Validation, Methodology, Investigation. Wenbo Shen: Funding acquisition, Methodology, Investigation. Zhanqi Cao: Formal analysis, Data curation, Methodology, Investigation. Chenyu Li: Formal analysis, Data curation, Methodology. Rubing Feng: Formal analysis, Data curation, Methodology. Puhui Xie: Supervision, Resources, Data curation, Methodology, Investigation, Conceptualization, Writing – review & editing. Fengqi Guo: Writing – review & editing, Resources, Methodology, Conceptualization.

Acknowledgement

The authors thank the financial support sponsored by Henan Provincial Key Science and Technology Project (262102111170), Natural Science Foundation of Henan Province (262300421680), and Postgraduate Education Reform and Quality Improvement Project of Henan Province (YJS2026XSJC23, YJS2025KC21).

Data Availability

The data supporting the findings of this study are available from the corresponding authors upon reasonable request.

References

1. Bonetta, S., Pignata, C., Bonetta, S., Amagliani, G., Brandi, G., Gilli, G., & Carraro, E. (2021). Comparison of UV, peracetic acid and sodium hypochlorite treatment in the disinfection of urban wastewater. *Pathogens*, *10*, 182. https://doi.org/10.3390/pathogens10020182
2. Cheng, X., Wang, S., Huang, W., Wang, F., Fang, S., Ge, R., Zhang, Q., Zhang, L., Du, W., Fang, F., Feng, Q., Cao, J., & Luo, J. (2022). Current status of hypochlorite technology on the wastewater treatment and sludge disposal: Performance, principals and prospects. *Science of the Total Environment*, *803*, 150085. https://doi.org/10.1016/j.scitotenv.2021.150085

3. Algwaiz, H. I. (2018). Cytological effects of bleaching agent (Quneex) on plant cells and plant DNA. *Pakistan Journal of Biological Sciences*, *21*, 205–214. https://doi.org/10.3923/pjbs.2018.205.214
4. Shen, S., Yuan, Y., Song, J., Zhu, Y., Wang, Y., Yue, C., Du, M., Wei, J., Feng, F., & Tian, M. (2025). A phenothiazine-based ratiometric fluorescent probe for detecting hypochlorite (ClO^-) and its application in foods and water samples. *Food Chemistry*, *485*, 144547. https://doi.org/10.1016/j.foodchem.2025.144547
5. Cao, S., Zhang, D., Teng, F., Liao, R., Cai, Z., Tao, Y., & Hu, H. (2021). Inhibitory effects of ultralow-dose sodium hypochlorite on Microcystis aeruginosa and Chlorella vulgaris: Differences in sensitivity and physiology. *Science of the Total Environment*, *774*, 145638. https://doi.org/10.1016/j.scitotenv.2021.145638
6. Liu, S. S., Yan, J. L., Wu, W. N., Zhao, X. L., Fan, Y. C., Wang, Y., & Xu, Z. H. (2022). Highly selective fluorescent probe for rapid turn-on detection and cell imaging of hypochlorite anion. *Journal of Photochemistry and Photobiology A: Chemistry*, *432*, 114082. https://doi.org/10.1016/j.jphotochem.2022.114082
7. Steinbeck, M. J., Nesti, L. J., Sharkey, P. F., & Parvizi, J. (2007). Myeloperoxidase and chlorinated peptides in osteoarthritis: potential biomarkers of the disease. *Journal of Orthopaedic Research*, *25*, 1128–1135. https://doi.org/10.1002/jor.20400
8. Winterbourn, C. C., Hampton, M. B., Livesey, J. H., & Kettle, A. J. (2006). Modeling the reactions of superoxide and myeloperoxidase in the neutrophil phagosome: Implications for microbial killing. *Journal of Biological Chemistry*, *281*, 39860–39869. https://doi.org/10.1074/jbc.M605898200
9. Hampton, M. B., Kettle, A. J., & Winterbourn, C. C. (1998). Inside the neutrophil phagosome: Oxidants, myeloperoxidase, and bacterial killing. *Blood*, *92*, 3007–3017. https://doi.org/10.1182/blood.V92.9.3007.421k47_3007_3017
10. Jurczyk, K., Nietzsche, S., Ender, C., Sculean, A., & Eick, S. (2016). In-vitro activity of sodium hypochlorite gel on bacteria associated with periodontitis. *Clinical Oral Investigations*, *20*, 1–9. https://doi.org/10.1007/s00784-016-1711-9
11. Jiang, Y., Wu, S., Jin, C., Wang, B., & Shen, J. (2018). Novel diaminomaleonitrile-based fluorescent probe for ratiometric detection and bioimaging of hypochlorite. *Sensors and Actuators B: Chemical*, *265*, 365–370. https://doi.org/10.1016/j.snb.2018.01.202
12. Stocker, P., Cassien, M., Vidal, N., Thetiot-Laurent, S., & Pietri, S. (2017). A fluorescent homogeneous assay for myeloperoxidase measurement in biological samples. A positive correlation between myeloperoxidase-generated HOCl level and oxidative status in STZ-diabetic rats. *Talanta*, *170*, 119–127. https://doi.org/10.1016/j.talanta.2017.03.102
13. Huang, Y., Gong, Z., Wu, M., Tan, Z., Ding, H., Ji, Y., Fan, C., Liu, G., & Pu, S. (2025). A novel AIEgen fluorescent probe based on quinoline-malononitrile for monitoring and imaging ClO^- and viscosity in biosystem. *Spectrochimica Acta Part A: Molecular and Biomolecular Spectroscopy*, *338*, 126176. https://doi.org/10.1016/j.saa.2025.126176

14. Momma, J., Takada, K., Suzuki, Y., & Tobe, M. (1986). Acute oral toxicity and ocular irritation of chemicals in bleaching agents. *Food Hygiene and Safety Science*, *27*, 553–560.
15. Thiruppathi, M., Thiyagarajan, N., Gopinathan, M., Chang, J. L., & Zen, J. M. (2017). A dually functional 4-aminophenylboronic acid dimer for voltammetric detection of hypochlorite, glucose and fructose. *Microchimica Acta*, *184*, 4073–4080. https://doi.org/10.1007/s00604-017-2440-8
16. Chen, P., Zheng, Z., Zhu, Y., Dong, Y., Wang, F., & Liang, G. (2017). Bioluminescent turn-on probe for sensing hypochlorite in vitro and in tumors. *Analytical Chemistry*, *89*, 5693–5696. https://doi.org/10.1021/acs.analchem.7b01103
17. Dodeigne, C., Thunus, L., & Lejeune, R. (2000). Chemiluminescence as diagnostic tool. A review. *Talanta*, *51*, 415–439. https://doi.org/10.1016/S0039-9140(99)00294-5
18. Ordeig, O., Mas, R., Gonzalo, J., Campo, D., Muñoz, F. J., F. J., & de Haro, C. (2005). Continuous detection of hypochlorous acid/hypochlorite for water quality monitoring and control. *Electroanalysis*, *17*, 1641–1648. https://doi.org/10.1002/elan.200403194
19. Kettle, A. J., Albrett, A. M., Chapman, A. L., Dickerhof, N., Forbes, L. V., Khalilova, I., & Turner, R. (2014). Measuring chlorine bleach in biology and medicine. *Biochimica et Biophysica Acta*, *1840*, 781–793. https://doi.org/10.1016/j.bbagen.2013.07.004
20. Wang, L., Li, W., Zhi, W., Ye, D., Zhang, W., & Ni, L. (2018). Rapid detection of hypochlorite by a coumarin-based hydrazide in aqueous solution and its application in live-cell imaging. *Sensors and Actuators B: Chemical*, *255*, 1112–1118. https://doi.org/10.1016/j.snb.2017.08.039
21. Tian, Y. M., Liu, G. B., Wu, W. N., Zhao, X. L., Han, X. F., Fan, Y. C., Wang, Y., & Xu, Z. H. (2023). A p-toluenesulfonamide-modified benzo[h]chromene hydrazone: Fluorescent turn-on detection of hypochlorite and its application to imaging the endoplasmic reticula of living cells and zebrafishes. *Spectrochimica Acta Part A: Molecular and Biomolecular Spectroscopy*, *296*, 122669. https://doi.org/10.1016/j.saa.2023.122669
22. Pan, Y., Liang, Z., Li, L., Yan, L., & Wu, X. (2024). A ratiometric fluorescent probe for selective detection of hypochlorite (ClO^-) and gallium (III) (Ga^{3+}) ions in environmental and food samples. *Spectrochimica Acta Part A: Molecular and Biomolecular Spectroscopy*, *323*, 124927. https://doi.org/10.1016/j.saa.2024.124927
23. Gao, G., Hao, C., Ding, C., Zheng, X., Liu, L., Xie, P., & Guo, F. (2023). A near-infrared colorimetric and fluorometric chemodosimeter for Cu^{2+} based on a bis-spirocyclic rhodamine and its application in imagings. *Research on Chemical Intermediates*, *49*, 1771–1783. https://doi.org/10.1007/s11164-022-04920-5
24. Suh, B., Kim, H., Jang, S., Kim, K. T., & Kim, C. (2022). A benzothiazole-based fluorescent and colorimetric probe for the detection of ClO^- and its application to zebrafish and water sample. *Spectrochimica Acta Part A: Molecular and Biomolecular Spectroscopy*, *270*, 120827. https://doi.org/10.1016/j.saa.2021.120827
25. Li, Y., He, Y., Ge, Y., Song, G., & Zhou, J. (2021). Smartphone-assisted visual ratio-fluorescence detection of hypochlorite based on copper nanoclusters. *Spectrochimica Acta Part A: Molecular and*

Biomolecular Spectroscopy, *255*, 119740. https://doi.org/10.1016/j.saa.2021.119740

26. Wang, G., Chen, K., Wang, H., Chen, C., & Wang, X. (2023). A smartphone-based visual ratiometric fluoroprobe for rapid and sensitive detection hypochlorous acid based on dual-emission metal organic frameworks. *Talanta*, *265*, 124897. https://doi.org/10.1016/j.talanta.2023.124897
27. Wang, X., Wang, X., Bai, Z., Ru, J., Zou, X., & Han, Q. (2024). Fluorescent imaging and smartphone detection of ClO^- using sensors based on trifluoromethylquinoline-substituted pyranonitrile. *Sensors and Actuators B: Chemical*, *402*, 135120. https://doi.org/10.1016/j.snb.2023.135120
28. Zang, L., Liang, C., Wang, Y., Bu, W., Sun, H., & Jiang, S. (2015). A highly specific pyrene-based fluorescent probe for hypochlorite and its application in cell imaging. *Sensors and Actuators B: Chemical*, *211*, 164–169. https://doi.org/10.1016/j.snb.2015.01.046
29. Nam, H., Batsaikhan, O., Park, S., Kim, K. T., & Kim, C. (2025). Easy and portable fluorescent probe for ClO^- detection in pure water: A versatile platform for environmental samples, bioimaging, and smartphone-assisted technologies. *Journal of Environmental Chemical Engineering*, *13*, 116804. https://doi.org/10.1016/j.jece.2025.116804
30. Shiraishi, Y., Yamada, C., & Hirai, T. (2019). A coumarin-dihydroperimidine dye as a fluorescent chemosensor for hypochlorite in 99% water. *RSC Advances*, *9*, 28636–28641. https://doi.org/10.1039/c9ra05533a
31. Kwon, N., Chen, Y., Chen, X., Kim, M. H., & Yoon, J. (2022). Recent progress on small molecule-based fluorescent imaging probes for hypochlorous acid (HOCl)/hypochlorite (OCl^-). *Dyes and Pigments*, *200*, (2022) 110132. https://doi.org/10.1016/j.dyepig.2022.110132
32. Ma, C., Zhong, G., Zhao, Y., Zhang, P., Fu, Y., & Shen, B. (2020). Recent development of synthetic probes for detection of hypochlorous acid/hypochlorite. *Spectrochimica Acta Part A: Molecular and Biomolecular Spectroscopy*, *240*, 118545. https://doi.org/10.1016/j.saa.2020.118545
33. zhang, H., Huo, F., Zhang, Y., & Yin, C. (2018). Mono- or di- naphthalimides as fluorophore to detect hypochlorous acid (HOCl) by ratiometric fluorescent signal and their biological application. *Sensors and Actuators B: Chemical*, *269*, 180–188. https://doi.org/10.1016/j.snb.2018.04.155
34. Savran, T. (2024). A new fluorene–based fluorescent probe for recognition of hypochlorite ions and its applications. *Journal of Fluorescence*, *34*, 1931–1943. https://doi.org/10.1007/s10895-024-03702-z
35. Gao, G., Zhao, B., Wang, S., Song, M., Xie, P., & Ru, G. X. (2026). A bifunctional fluorescence probe for dual-channel real-time monitoring of nitric oxide and viscosity during cadmium stress in plants. *Microchemical Journal*, *224*, 117529. https://doi.org/10.1016/j.microc.2026.117529
36. Kim, E., Choi, B., Kim, S., Lee, J. J., & Kim, C. (2025). Easy and fast detection of hypochlorite by a bithiophene-based fluorescent turn-on sensor and its applications to test strips, real water samples, and smartphone-assisted platform. *Journal of Fluorescence*, *35*, 7809–7819. https://doi.org/10.1007/s10895-024-04123-8
37. Song, Z., Mao, D., Sung, S. H. P., Kwok, R. T. K., Lam, J. W. Y., Kong, D., Ding, D., & Tang, B. Z. (2016). Activatable fluorescent nanoprobe with aggregation-induced emission characteristics for selective

in vivo imaging of elevated peroxynitrite generation. *Advanced Materials*, *28*, 7249–7256. https://doi.org/10.1002/adma.201601214

38. Xie, P., Guo, F., Gao, G., Fan, W., Yang, G., & Xie, L. (2016). A near-infrared fluorescent chemodosimeter for ratiometric detecting fluoride based on desilylation reaction. *Journal of Fluorescence*, *26*, 1737–1742. https://doi.org/10.1007/s10895-016-1865-5
39. Wang, Y., Xia, J., Han, J., Bao, X., Li, Y., Tang, X., Ni, L., Wang, L., & Gao, M. (2016). A fast-responsive fluorescent probe based on BODIPY dye for sensitive detection of hypochlorite and its application in real water samples. *Talanta*, *161*, 847–853. https://doi.org/10.1016/j.talanta.2016.09.025
40. Feng, H., Zhang, Z., Meng, Q., Jia, H., Wang, Y., & Zhang, R. (2018). Rapid response fluorescence probe enabled in vivo diagnosis and assessing treatment response of hypochlorous acid-mediated rheumatoid arthritis. *Science Advances*, *58*, 1800397. https://doi.org/10.1002/advs.201800397
41. Li, X., Han, Y., Sun, S., Shan, D., Ma, X., He, G., Mergu, N., Park, J. S., Kim, C. H., & Son, Y. A. (2020). A diaminomaleonitrile-appended BODIPY chemosensor for the selective detection of Cu^{2+} via oxidative cyclization and imaging in SiHa cells and zebrafish. *Spectrochimica Acta Part A: Molecular and Biomolecular Spectroscopy*, *233*, 118179. https://doi.org/10.1016/j.saa.2020.118179
42. Zheng, X., Wang, G., Liu, L., Li, X., Xie, P., Fan, Y., Cao, Z., Niu, C., Tian, D., & Xie, L. (2025). Hydrogen bonding-induced multicolor and thermochromic emissions of triphenylamines. *Chemistry - A European Journal*, *31*, e202500643. https://doi.org/10.1002/chem.202500643
43. Song, X., Wang, Y., Ru, J., Yang, Y., Feng, Y., Cao, C., Wang, K., Zhang, G., & Liu, W. (2020). A mitochondrial-targeted red fluorescent probe for detecting endogenous H_2S in cells with high selectivity and development of a visual paper-based sensing platform. *Sensors and Actuators B: Chemical*, *312*, 127982. https://doi.org/10.1016/j.snb.2020.127982
44. Duan, N., Feng, J., Deng, B., Yang, S., Tian, H., & Sun, B. (2022). A colourimetric fluorescent probe for the sensitive detection of total iron in wine. *Food Chemistry*, *383*, 132594. https://doi.org/10.1016/j.foodchem.2022.132594

Table

Table 1 is available in the Supplementary Files section.

Scheme

Scheme 1 is available in the Supplementary Files section.

Figures

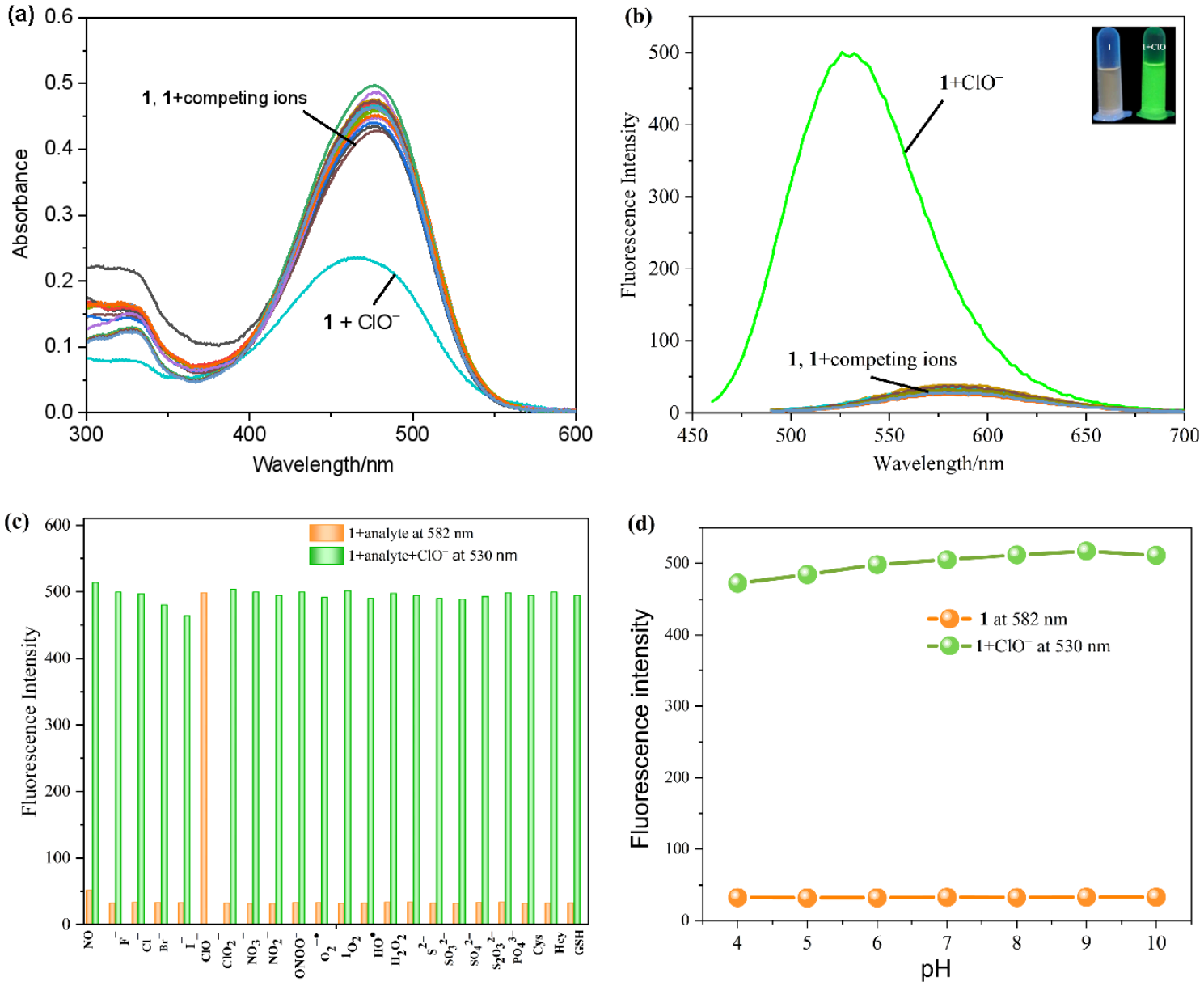


Figure 1

(a) Absorption and (b) fluorescence spectra of 1 (10 μM) in presence of an analyte (100 μM) (l_{ex}: 410 nm for 1 + ClO^-, 480 nm for 1, and 1 + other analytes. Insert: photographs of 1 and 1 + ClO^- under 365 nm light). (c) Maximum fluorescence intensities of 1 (10 μM) in presence of an analyte (100 μM) (Red). Fluorescence intensities of 1 (10 μM) at 530 nm in presence of an analyte (100 μM) and further addition of ClO^- (100 μM) (green), (d) Fluorescence intensities of 1, 1 (10 μM) with ClO^- (100 μM) *in EtOH*-H_2O *(1:1, v/v)* at pH 4-10.

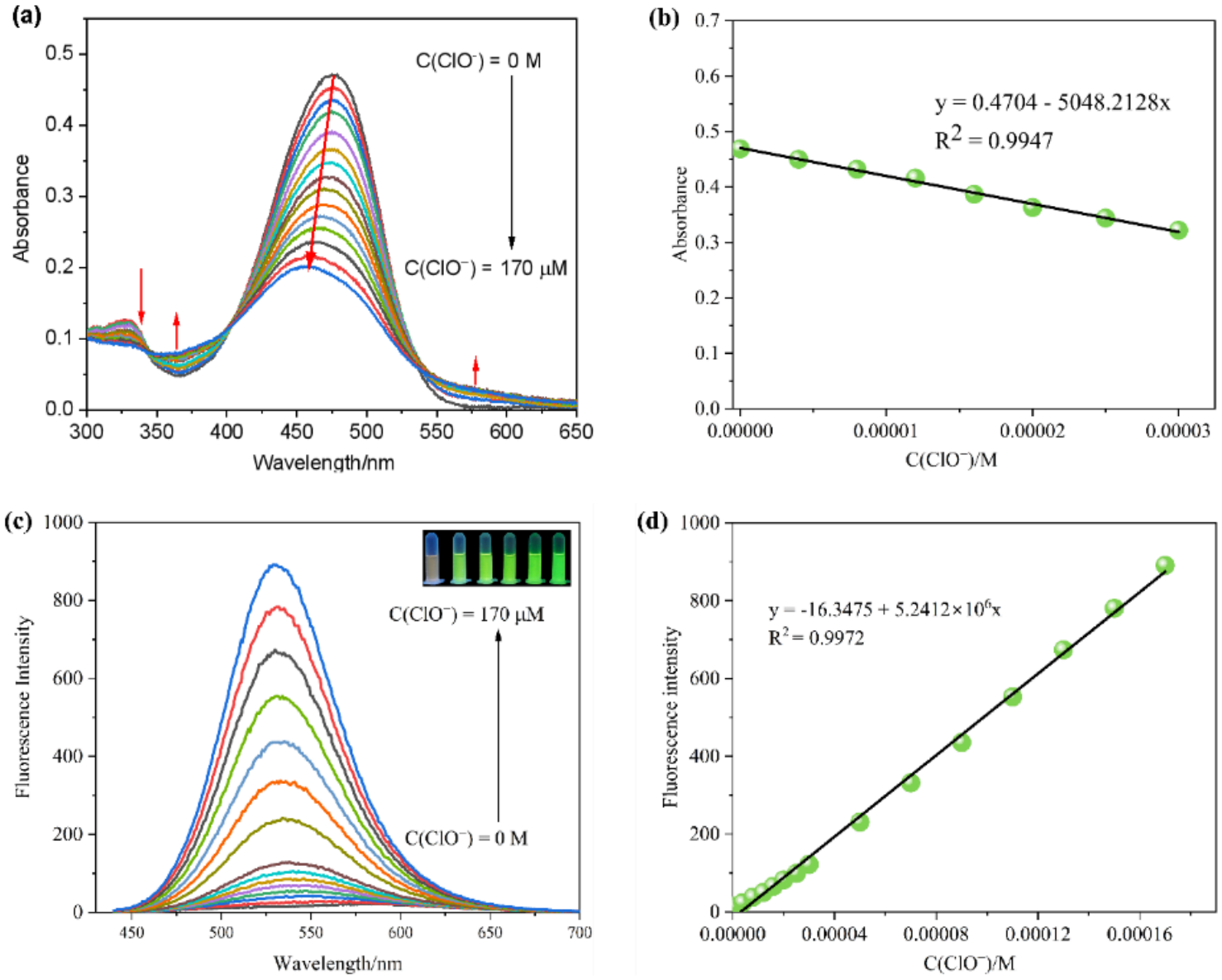


Figure 2

(a) Absorption spectra of probe **1** (10 μM) with ClO^-. **(b)** The linear fitting of absorbance at 480 nm. **(c)** Fluorescence spectra of probe **1** (10 μM) with ClO^- (λ_{ex}= 410 nm). **(d)** The linear fitting of fluorescence intensity at 530 nm.

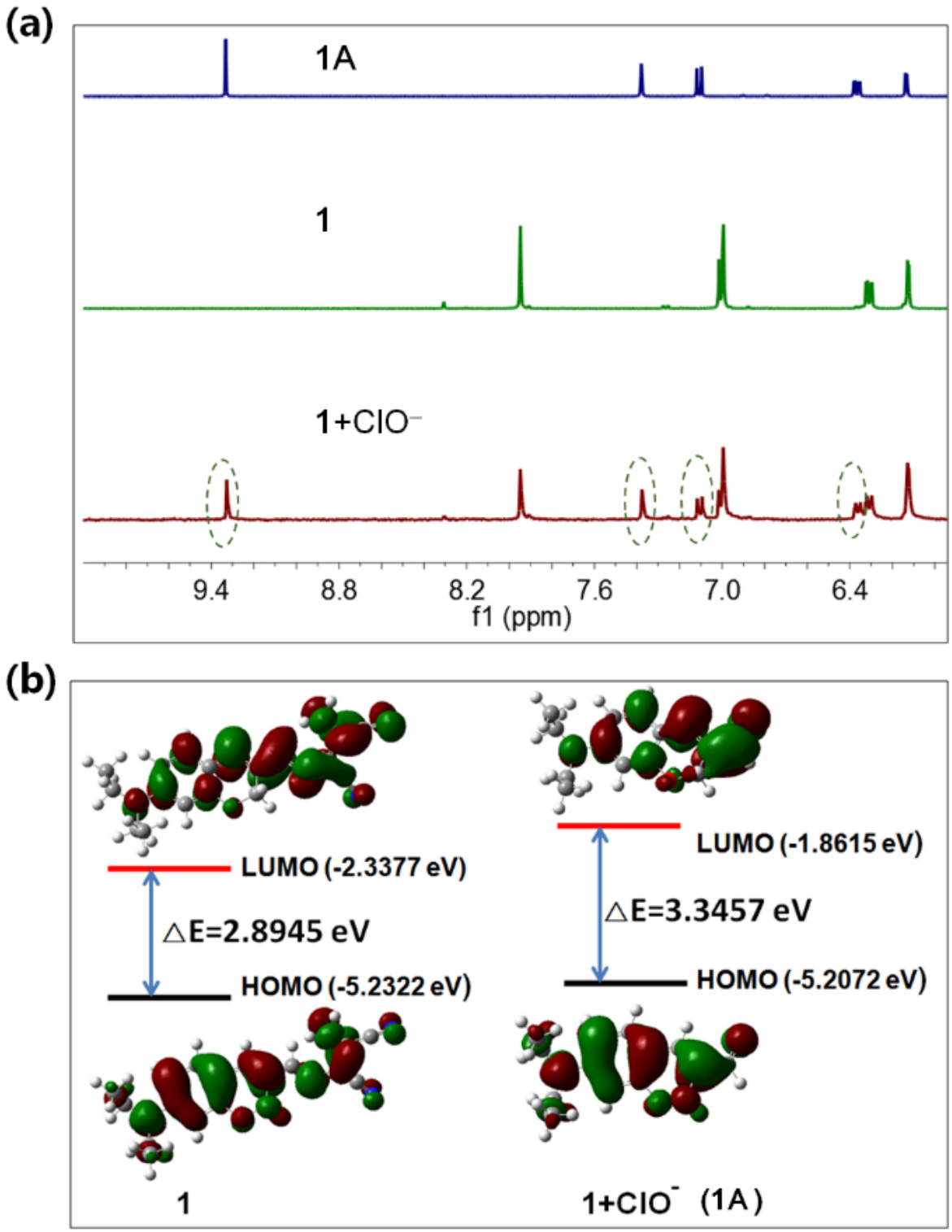


Figure 3

(a) Partial ^{1}H NMR spectra of **1** (green), the mixture of **1** + ClO^- (red), and the compound **1A** (purple). **(b)** Energy diagrams of HOMO and LUMO orbitals for **1**, **1** + ClO^- (**1A)** by DFT calculation.

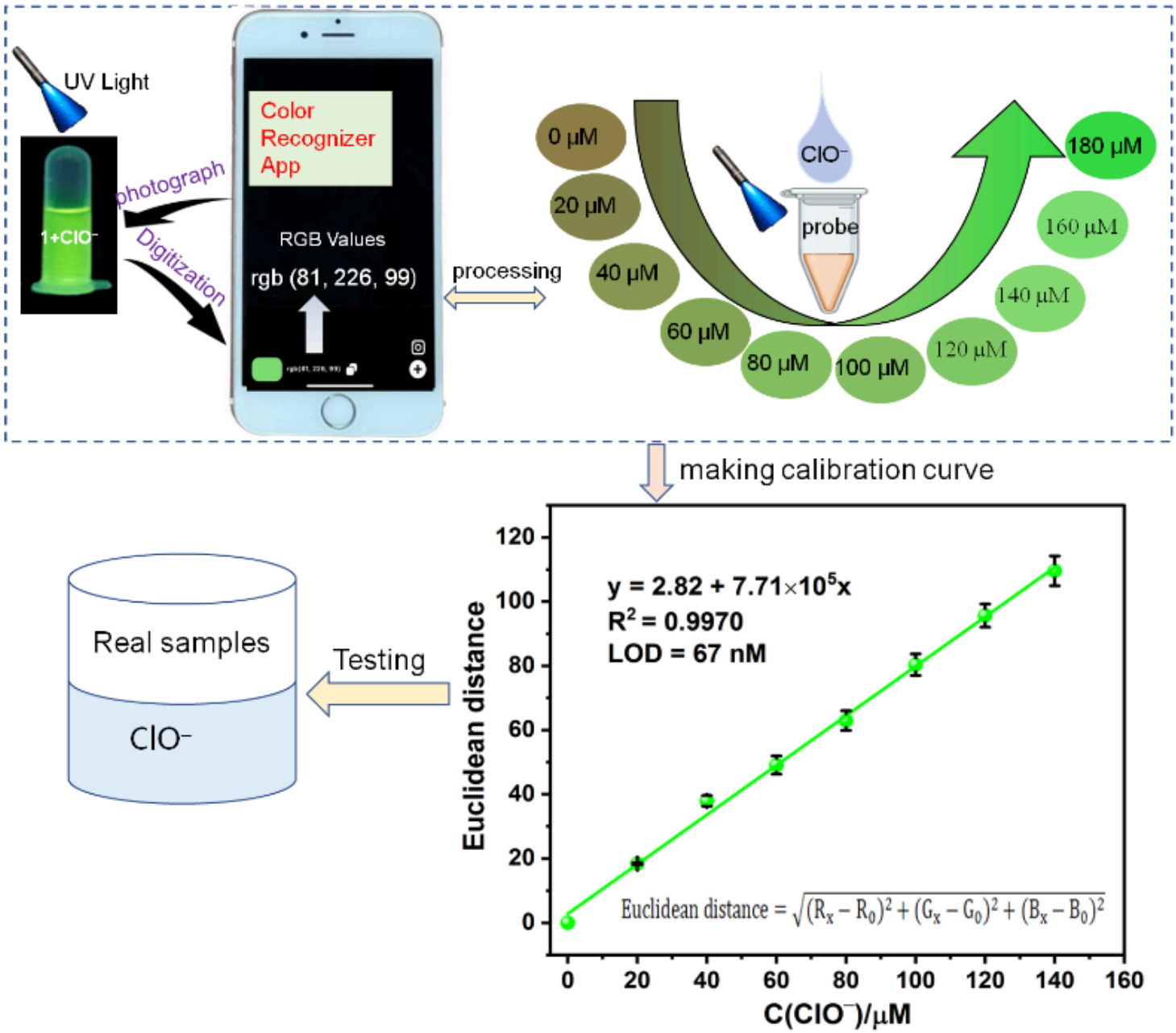


Figure 4

The detection of ClO^- (0–180 μM) by probe **1** (10 μM) in conjunction with a smartphone application and linear calibration curve between the Euclidean distance and the concentrations of ClO^-. Error bars: SE, n=3.

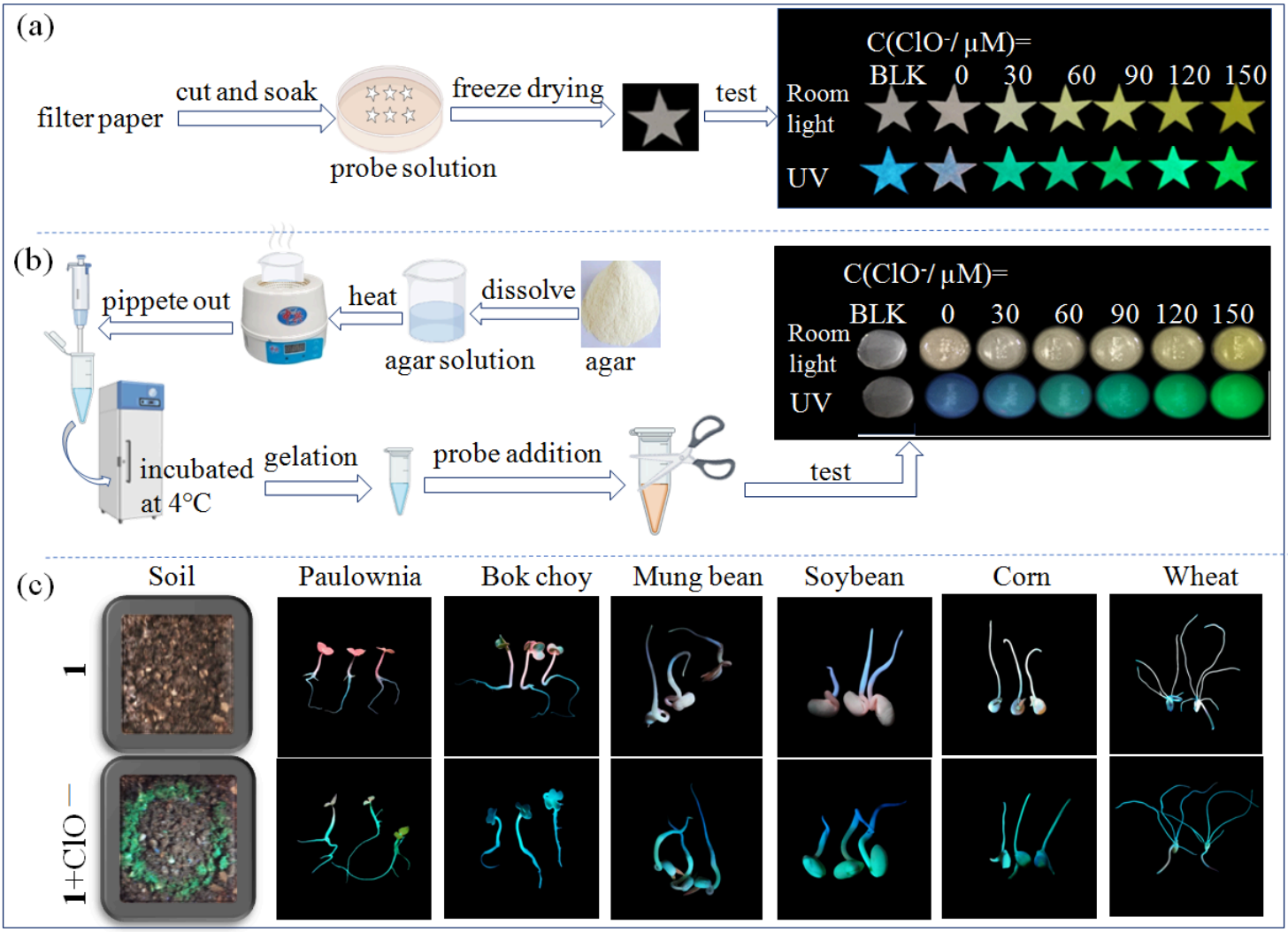


Figure 5

Schemes and images (ambient/UV light) of probe 1 embedded test strips (a) and agarose gel films (b) exposed to increasing ClO^- **concentrations (0–150 μM). (c)** Fluorescent images about sensoring ClO^- using probe **1** in soil and plant seedings.

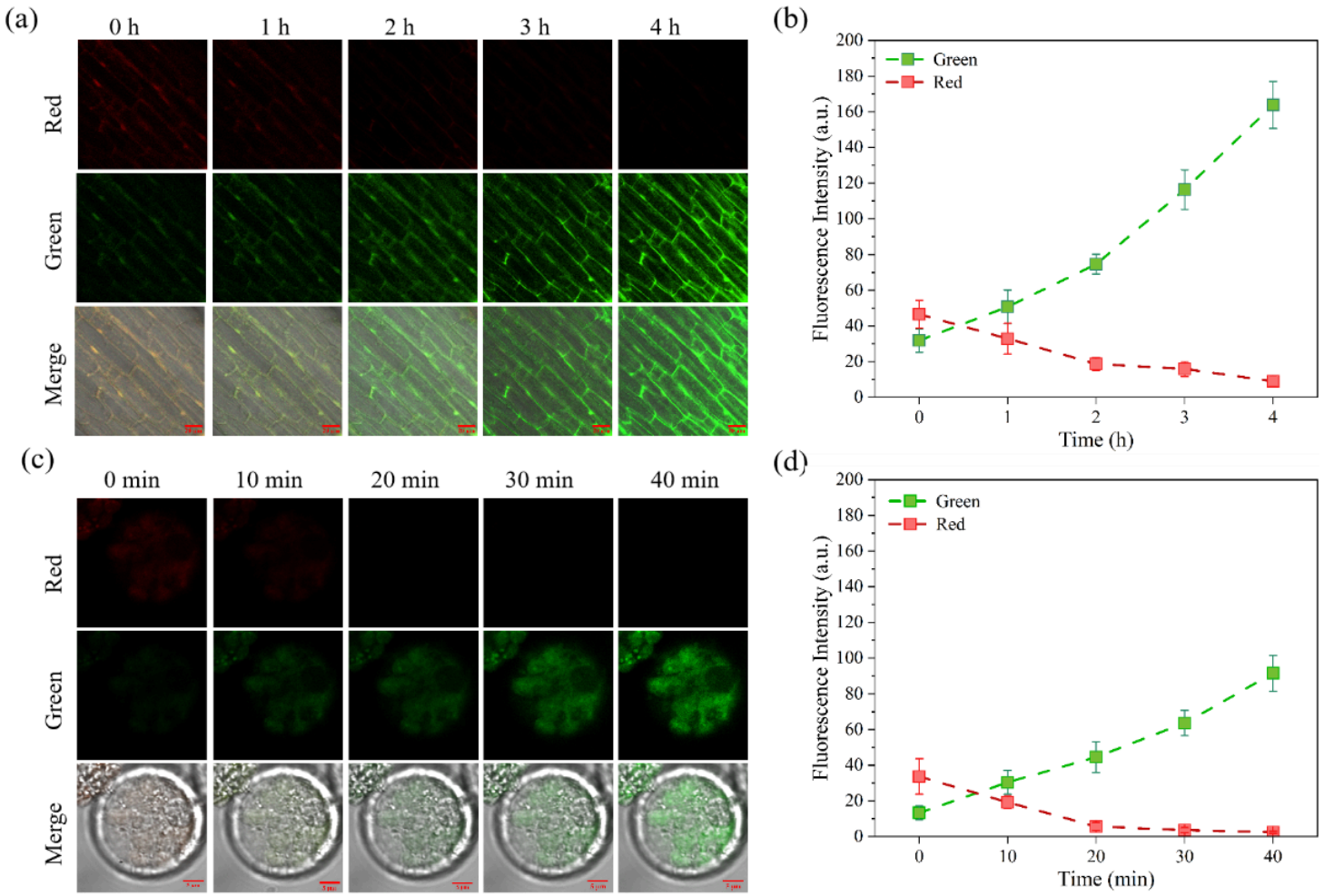


Figure 6

(a) Time-dependent fluorescence imaging of probe **1** (10 μM) for exogenous NaClO in the root tip cells of *Paulownia*. Scale bar: 20 μm. **(b)** The relative fluorescence intensity data output of Figure 6a. Data are mean ± SD. **(c)** Time-dependentfluorescence imaging of probe **1** (10 μM) for exogenous NaClO (100 μM) in *Paulownia* leaf protoplasts. Scale bar: 5 μm. **(d)**The relative fluorescence intensity data output diagram of Figure 6c. Data are mean ± SD.

Supplementary Files

This is a list of supplementary files associated with this preprint. Click to download.

- SupportingMaterials1.docx
- Table1.docx
- Scheme1.docx